

Single-Step Synthesis and Surface Plasmons of Bismuth-Coated Spherical to Hexagonal Silver Nanoparticles in Dichroic Ag:Bismuth Glass Nanocomposites

Shiv Prakash Singh · Basudeb Karmakar

Received: 1 September 2010 / Accepted: 23 February 2011 / Published online: 22 March 2011
© Springer Science+Business Media, LLC 2011

Abstract Here, we report for the first time the synthesis of bismuth-coated silver nanoparticles in dichroic bismuth glass nanocomposites by a novel and simple one-step melt quench technique without using any external reducing agent. The metallic silver nanoparticles (Ag NPs) were generated first, and subsequently, metallic bismuth was deposited on the Ag NPs and formed a thick layer. The reduction of Bi^{3+} to Bi^0 and subsequently its deposition on the Ag NPs (which were formed earlier than Bi^0) in the $\text{K}_2\text{O}-\text{Bi}_2\text{O}_3-\text{B}_2\text{O}_3$ (KBB) glass system have been explained by their standard reduction potentials. The UV–vis absorption spectra show a prominent surface plasmon resonance (SPR) absorption band at 575 nm at lower concentrations (up to 0.01 wt%); three bands at 569, 624 and 780 nm at medium concentration (0.02–0.03 wt%); and two weak bands at 619 and 817 nm at highest concentration (0.06 wt%) of silver. They have been explained by the electrodynamic theories. TEM images reveal the conversion of spheroidal (5–15 nm) to hexagonal (10–35 nm) shaped Ag NPs with the increase in concentration of silver (up to 0.06 wt%). SAED pattern confirms the crystalline planes of rhombohedral bismuth and cubic silver. Thermal treatment at 360 °C, which is the glass transformation temperature (T_g) of the sample containing lower concentration of silver (0.007 wt%), shows red-shifted SPR band due to increase in size of NPs. Whereas the sample containing higher concentration (0.06 wt%) of silver under similar treatment exhibited changes in SPR spectral profile happened due to

conversion to spherical NPs from hexagonal shape and reduction in size (10–20 nm) of NPs after heat treatment for 65 h. HRTEM images corroborate the different orientations of the NPs. FESEM images reveal hexagonal disk like structure having different orientations. Dichroic nature of the nanocomposites has been explained with the size and shape of Ag nanoparticles. We believe that this work will create new avenues in the area of nanometal–glass hybrid nanocomposites and the materials have significant applications in the field of optoelectronics and nanophotonics.

Keywords Surface plasmon resonance · Nanocomposites · Hexagonal nanoparticle · Bismuth glass · Silver

Introduction

The study of the nanoparticles (NPs) is the emerging field which has enormous potential for advanced research in the twenty-first century. The electrons of conduction band of the nanoparticle interact with the various forms of energy (i.e., light, electrical, magnetic, etc.) and show very interesting results which are not shown by its bulk form. When particular wavelength of electromagnetic radiation interacts with a nanoparticle to create a coherent oscillation of the conduction electrons, it is termed as a surface plasmon resonance (SPR) of that NP [1–5]. The study of plasmonic properties of the noble metal nanoparticles has been fascinated interests of various researchers as a result of their various applications such as waveguide [6, 7], photonics circuits [8–12], and sensors [13–15]. All of these applications are based on the localized surface plasmon resonance (LSPR) of the nanoparticle which has emerged into a new area of nanophotonics called plasmonics. The

S. P. Singh · B. Karmakar (✉)
Glass Science and Technology Section, Glass Division Central
Glass and Ceramic Research Institute (CSIR, India),
196 Raja S.C. Mullick Road,
Kolkata 700 032, West Bengal, India
e-mail: basudebk@cgeri.res.in

LSPR results in the selective photon absorption and scattering which allows the optical properties of the nanoparticles to be monitored by conventional UV–vis spectroscopy. The SPR band strongly depends on the shape, size, distribution and concentration of the metal clusters. Any techniques allowing manipulation of the abovementioned parameters of such nanocomposite materials in a controlled way are very promising in view of their applications in the field of nanophotonics; this includes manufacturing of nonlinear materials, nanodevices, optical elements, etc. The observation of multiple plasmon peaks is another feature of interest for the LSPR spectra of spherical, nanorods, triangular nanoprisms, hexagonal and nanocubes [1–5]. These are developed either by multipolar excitation or by interaction with the environment, such as with an asymmetric dielectric environment or with other nearby metal particles.

Nanomaterials composed of both noble metals, such as platinum, gold and silver, have strong LSPR effects, like strong absorption ranges from the visible to near-infrared (NIR) region, are generally considered, and they exhibit facile surface functionalization chemistry. These properties make them excellent test beds for both fundamental studies and technological advances in the fields ranging from nanobiodevices to catalysis. The electronic confinement in silver nanoparticles induces dramatic changes in the optical properties. These changes are caused by SPR that come from the electromagnetic (EM) field excitation inside the particles associated with the collective oscillation of the electrons. Interactions between closely spaced metallic nanoparticles shift the frequency of the SPR through EM coupling. These interactions induce different spectral responses depending on the light polarization with anisotropic local surroundings.

The synthesis of nanometals is generally carried out by multi-step sol–gel, ion implantation, pulsed laser deposition, ion exchange methods, etc. [2, 16–19] in various dielectric media including glass. But in situ generation of nanometals in glass dielectric by single-step methodology is very difficult. As glass is a highly transparent material which is thermally and chemically stable, therefore, it is a promising dielectric medium for encapsulation of various nanometals. Again, glass is itself a very smart material for technology as well as academic aspect due to their inherent superiority over other dielectric. So, the study of nanometal-embedded glass nanocomposites is a very important and interesting subject and need to explore its novel preparative methods and properties. It has been an increasing interest in the synthesis of heavy metal oxide (HMO) glasses due to their high refractive index, low phonon energy and high density [20, 21]. Bismuth-based HMO glasses exhibit large third-order nonlinear optical susceptibility and are important candidates for optic and

optoelectronic components [22, 23]. The synthesis of nanoparticles of various metals such as silver, gold, platinum etc. in the bismuth glass is very difficult as bismuth has tendency to reduce itself to metallic bismuth by autothermo reduction at high melting temperature. It is known that glasses embedded with metal nanoparticles may exhibit different colors, depending on whether they are viewed in transmission or reflection lights. This phenomenon termed as dichroic which exhibits different colors at different angles [11, 24].

In this paper, we demonstrated a novel one-step melt quench synthesis method of the bismuth-coated spherical and hexagonal silver nanoparticles in the bismuth glass matrix. The optical properties have been evaluated by using the UV–vis spectroscopy. The changes in the shape and size of bismuth-coated silver nanoparticles were studied by TEM, SAED, HRTEM and FESEM images. The thermal effects on the shape and size of the bismuth-coated silver nanoparticles and their SPR bands are also demonstrated here.

Experimental Section

Synthesis Procedure

The raw materials used were potassium carbonate, K_2CO_3 (GR, 99.9%, Loba Chemie), bismuth (III) oxide, Bi_2O_3 (99%, Loba Chemie), orthoboric acid, H_3BO_3 (GR, 99.5%, Loba Chemie) and silver nitrate, $AgNO_3$ (99.9%, Exceller, Qualigens). These raw materials were used without further purification. All the raw materials were mixed thoroughly in isopropyl alcohol medium in an agate mortar followed by drying. Twenty-five-gram glass of composition (mol%) $30K_2O-40Bi_2O_3-30B_2O_3$ (KBB) was prepared using above mixed raw materials in a high purity silica crucible at 1,100 °C in air for 10 min in a raising hearth electric furnace followed by intermittent stirring of 0.5 min. The molten glass was cast onto a carbon plate and annealed at 350 °C for 2 h. The Ag^0 -doped nanocomposites were prepared in a similar technique using respective dopant concentrations (in excess) and identified as G, NC1, NC2, NC3, NC4 and NC5. The compositions are given in Table 1. The melting and annealing times were kept constant for all the above samples. Samples of about 5.0 ± 0.01 mm thickness for optical absorption measurements were prepared by cutting, grinding, and polishing with cerium oxide powder. The density was measured by the Archimedes method using distilled water as immersion liquid with an error of $\pm 0.7\%$. The heat treatment of the samples doped with 0.007 and 0.03 wt% of silver was carried out at 360 °C for different duration in air.

Table 1 Composition and some properties of the investigated nanocomposites

Sample identity	Concentration of silver (wt%) ^a	Density (g cm ⁻³)	Color of transmitted light	Color of reflected light	SPR peak position (±1, nm)
G	0	5.201	Brown	Brown	500–700
NC1	0.007	5.229	Light blue	Brown	575
NC2	0.01	5.249	Blue	Brown	575
NC3	0.02	5.281	Blue	Brown	569, 624, 780
NC4	0.03	5.290	Blue	Brown	569, 624, 780
NC5	0.06	5.304	Blue	Brown	619, 817

All Ag concentrations are in excess

^a Base glass composition (mol%): 30K₂O–40Bi₂O₃–30B₂O₃

Characterization

The prepared samples were characterized using following instruments. The X-ray diffraction patterns of the bulk samples were recorded in an X’pert Pro MPD diffractometer (PANalytical) operating at 40 kV and 30 mA using Ni-filtered CuKα radiation with the X’celerator with step size 0.05° (2θ) step time 0.5 s, from 5° to 90°. TEM and SAED were done using a FEI instrument (Tehnai-30, ST G²) operating at an accelerating voltage of 300 kV. The UV–vis transmission spectra were obtained with a double-beam spectrophotometer (Lambda 20, Perkin-Elmer). The uncertainty of the band position was ±0.1 nm. FESEM photomicrographs were recorded with a Gemini Zeiss Supra™ 35VP Model (Carl Zeiss) instrument using an accelerating voltage of 4.9 kV. The samples for FESEM experiment were prepared by etching in 2-wt% HF aqueous solution for 2 min.

Results and Discussion

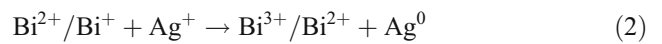
Synthesis of Bismuth-Coated Silver Nanoparticles in Bismuth Glass

The metal–glass nanocomposites were prepared by doping 0, 0.007, 0.01, 0.02, 0.03 and 0.06 wt% (in excess) of silver in the potassium bismuth borate, K₂O–Bi₂O₃–B₂O₃ (KBB) glass matrix. Their composition and some properties are given in Table 1. The Bi³⁺ ions of bismuth trioxide (Bi₂O₃) at higher melting temperature (>1,000 °C), disproportionate to its lower valence state by the autothermo reduction as follows [20, 21]:



Here, Ag has been doped in the bismuth glasses for the formation of the silver–bismuth bimetallic nanoparticles and to study their optical properties. The silver ions (Ag⁺)

get reduced to metallic silver (Ag⁰) in the presence of lower state of Bi³⁺ as shown below.



The standard reduction potential of various species involved in these reactions are given in Table 2 [25]. From the reduction potential data, it is quite clear that the silver ion (Ag⁺) has higher reduction potential than that of bismuth ion (Bi³⁺). The standard Gibbs free energy (ΔG⁰=–nFE⁰) has also been calculated by using standard reduction potential from Eq. (1) and (2), and it is found that Bi³⁺/Bi⁰ is –89 kJ and Ag⁺/Ag⁰ is –77 kJ. So, from the above data of standard reduction potential and free energy, it is evident that the silver ion would reduce first than that of bismuth ion. Consequently, bismuth-coated silver nanoparticles were obtained. This phenomenon along with other feature involved in this study is shown schematically in Fig. 1.

Figure 2 shows the X-ray diffraction patterns of the glasses. All the glasses have shown amorphous-like nature with a very weak peak at 2θ=27.56°. This is the characteristic peak of <012> hkl plane of rhombohedral metallic bismuth (JCPDS file no. 85-1331) which was reduced by autothermo reduction during melting process at 1,100 °C.

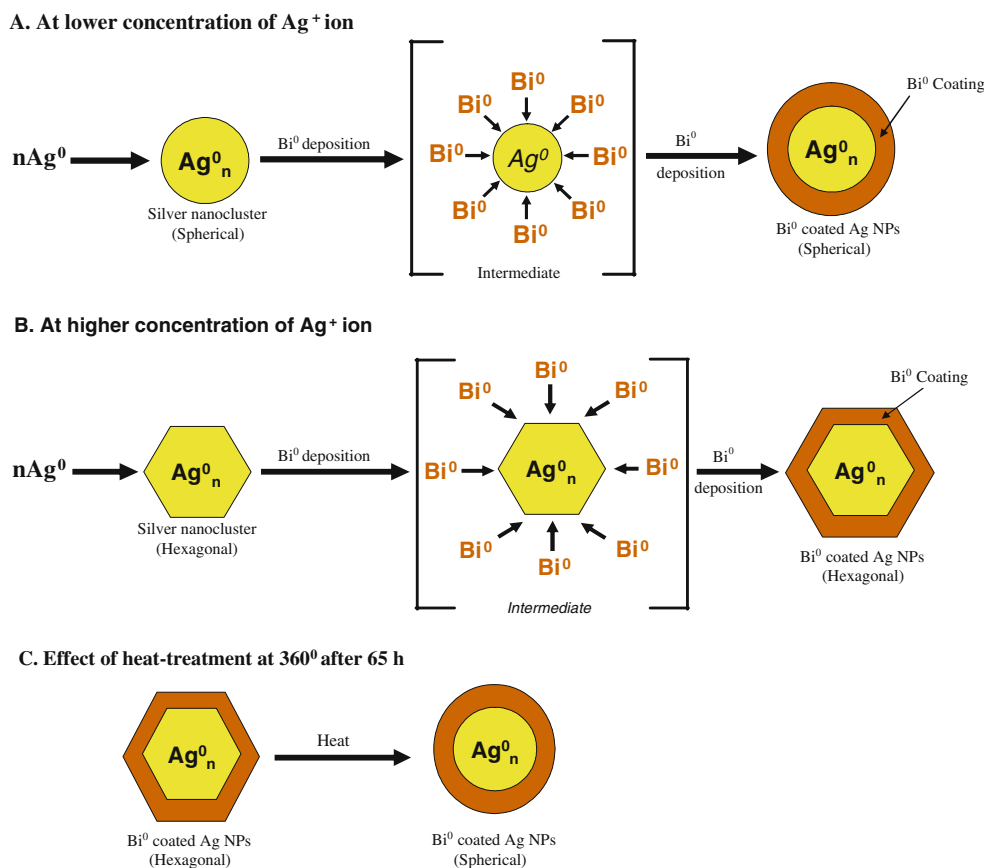
Figures 3 and 4 show the TEM images for the samples NC1 and NC4 of potassium bismuth borate (KBB) glasses doped with 0.007 (NC1) and 0.03 (NC4) wt% of Ag.

Table 2 Standard reduction potential of silver and bismuth species

Redox reaction	Standard reduction potential (E ⁰ , V)
Ag ⁺ /Ag ⁰	0.80
Bi ⁺ /Bi ⁰	0.50
Bi ³⁺ /Bi ⁰	0.31
Bi ³⁺ /Bi ⁺	0.20
Bi ³⁺ /Bi ²⁺	< 0.20 ^a

^a Exact value is not available

Fig. 1 (Color online) Schematic representation of synthesis of Bi⁰-coated Ag⁰ NPs at (a) lower and (b) higher concentrations of Ag⁺, and (c) effect of heat treatment on the hexagonal-shaped Bi⁰-coated Ag⁰ NPs



Equations 1 and 2 indicate that the bismuth was reduced in the presence of silver nanoparticles which have reduced earlier (as Ag⁰ has higher reduction potential than Bi⁰). The TEM images of NC1 (see Table 1) glass show spheroidal nanoparticle of size range 5–15 nm, whereas the NC4 (see Table 1) glass show hexagonal-shaped nanoparticles of size range 10–35 nm, and aspect ratio ranges from 1.2 to 1.6.

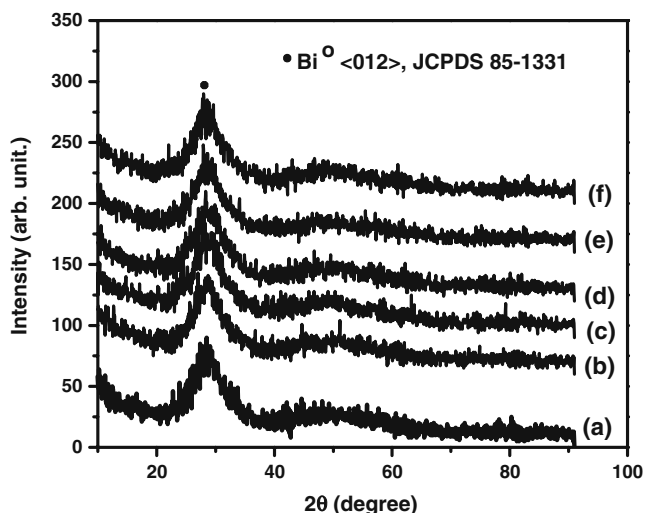


Fig. 2 XRD spectra of (a) G, (b) NC1, (c) NC2, (d) NC3, (e) NC4 and (f) NC5 (see Table 1 for composition)

This indicates that the shape of Ag NPs becomes hexagonal at higher concentration of silver (0.03 wt%). These changes in shape of NPs are also shown in Fig. 1. Figures 3b and 4b show the SAED patterns of distinct hkl crystalline planes of <012> and <111> of rhombohedral bismuth (JCPDS file no. 85-1331) and cubic silver (JCPDS file no. 01-1667) for both the samples, respectively. Lattice-resolved high resolution transmission electron microscopy (HRTEM) images of <101> and <012> hkl planes for the NC1 and NC4 glass nanocomposites have shown in Figs. 3c and 4c, respectively. From the lattice plane analysis, it is revealed that these planes are of metallic rhombohedral bismuth (JCPDS file no. 85-1331). But from TEM image analysis, there is no evidence for development of silver–bismuth core-shell NPs. XRD and SAED patterns are also not demonstrating any type of crystalline plane for silver–bismuth bimetallic alloy. Ould-Elt et al. [26] have shown hexagonal images of bismuth–nickel bimetallic nanoparticles when their diameter exceeds 10 nm. They have also ruled out the presence of pure bismuth phase or nickel phase since the lattice planes of those compounds do not matched with the SAED patterns. Therefore, it is clear from the standard reduction potential (E^0) data that the reduction to metallic silver nanoparticles is faster than that of bismuth and finally silver NPs being coated by the bismuth thick layers. These

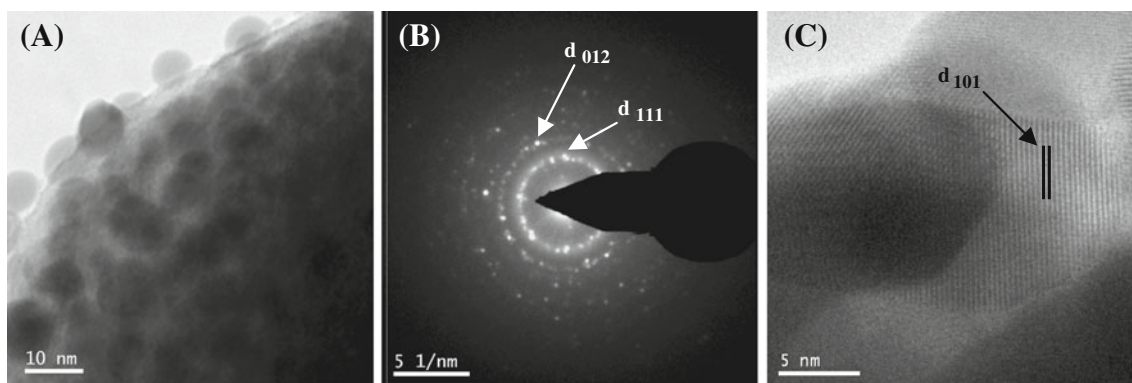


Fig. 3 **a** TEM image of the nanocomposites NC1, **b** their SAED, and **c** HRTEM images (see Table 1 for composition)

types of coating by deposition of one metal layer on the other metal nanoparticles are also reported in the literature [27–29]. The similar observation has also been reported by Gutiérrez et al. [27] where bismuth was reduced and deposited on the silver NPs. Likewise, Katsikas et al. [28] have reported for silver and mercury. They have added various concentrations of $\text{Hg}(\text{ClO}_4)_2$ to a silver sol and all metal ions reduced until no further changes in the absorption spectrum occurred. It is pointed out that the silver plasmon band was blue-shifted, which is taken as an indication that mercury was deposited on the silver particles. Moore et al. [30] have also reported hexagonal-shaped Bi–Te nanocrystal ceramic nanocomposites on high metal loading from mixed-metal oxides.

The microstructures of the resultant glasses have been examined by FESEM image analysis. Figure 5 shows nanostructures of 0.03 wt% silver-doped glasses. The glass doped with 0.03 wt% of silver demonstrated house-of-disk (hexagonal-shaped) nanostructure. Sun et al. [31] have also find similar SEM images for silver nanoplates on GaAs substrates. This fact is also supported by the TEM images. These hexagonal disk images show various orientations.

The glasses show dichroic property with the increase in the concentration of silver which has enormous application

in the field of dichroic polarizer, coating, sensor, etc. [32]. From literature, it is seen that there is no clear explanation for the dichroic nature. Researchers have found that soda lime silicate glasses in the presence of reducing agents, gold ions (Au^{3+}), on heat treatment at high temperature demonstrate dichroic behavior. They attributed the dichroic nature to the formation of smaller and larger gold particle formation [32]. Magruder et al. have demonstrated the dichroism by Ag NPs in fused silica by bimodal size distribution [33]. But here in this case, gradual change in shape and size of the NPs with the silver concentration may be responsible for dichroic nature. Figure 6 shows photographs of the glass containing 0.06 wt% of silver. The glasses show dichroic property, i.e., brown color in reflection and sky blue color in the transmission mode of view in all the silver-containing nanocomposites. The gradual change of size (increasing) and shape (spherical to hexagonal) of the nanoparticles, which has been explained above, are clearly exhibited in gradual alteration of colors in reflected and transmitted lights of the nanocomposites. Moreover, Fig. 7 shows various orientations of lattice planes in different directions with respect to each other. The hexagonal plates show various orientations in different direction (see Fig. 5). These different orientations support

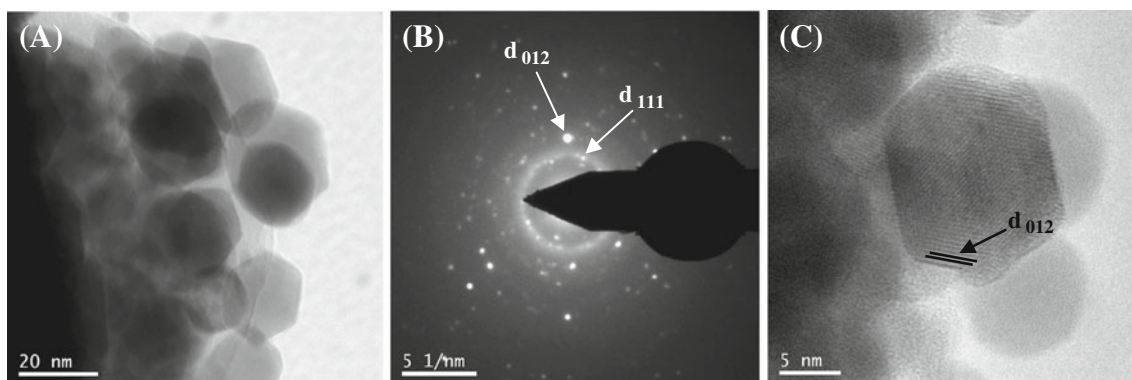
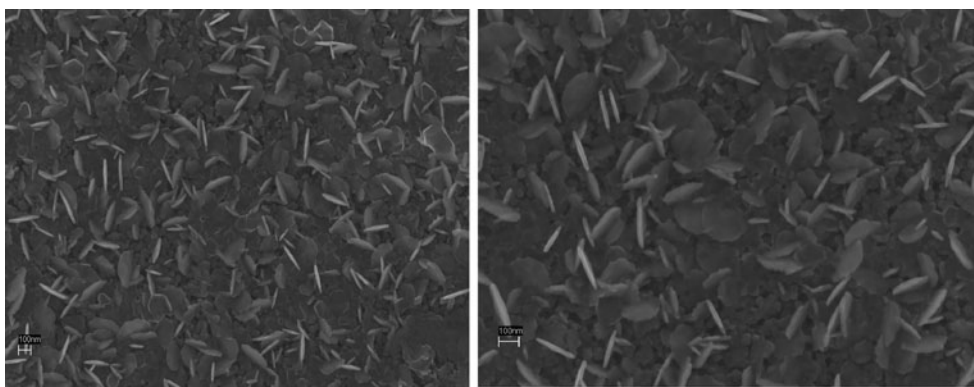


Fig. 4 **a** TEM image of the nanocomposites NC4 showing hexagonal-shaped Bi-coated Ag NPs having an aspect ratio of 1.2–1.6, **b** SAED images of Bi-coated Ag NPs, and **c** their HRTEM images (see Table 1 for composition)

Fig. 5 FESEM photomicrographs of the nanocomposite NC4 (see Table 1 for composition)



the dichroic nature of the glass. These observations may be correlated with the dichroic property of the glass as it can rotate the light in different direction. Therefore, it causes different color appearance when viewed from different angles.

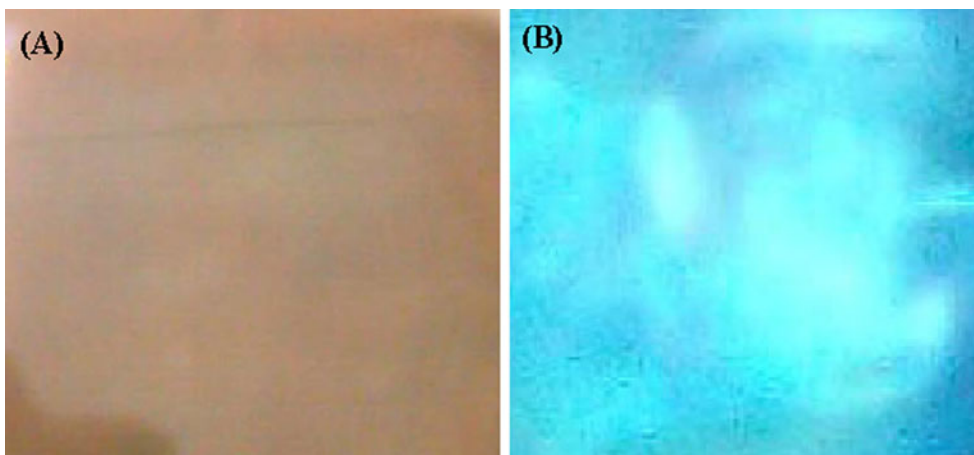
It is now well established that the colors of nanoparticles of various metal in terms of strong absorption bands in the visible region of the spectrum caused by their surface plasmon resonance (SPR). The SPR is due to extensive electronic correlation and corresponds to a collective excitation of weakly bound electrons relative to the ionic cores, i.e., the correlated motion of the cluster's peripatetic electrons in the attractive field due to the positively charged ionic cores. Mie [34] developed a classical electrodynamical model to quantify the collective excitation of electrons in metallic nanoparticles [35, 36]. A similar approach by the Drude model has also been applied to metal nanoparticles.

According to Mie theory, the absorption cross-section, $\sigma(\nu)$ (where ν is the frequency of the incident light) of a nanoparticle embedded in a medium of known dielectric constant, ϵ_m , is given by

$$\sigma(\nu) = 4\pi\nu \text{Im}[\alpha(\nu)]/c\epsilon_m^{1/2} \quad (3)$$

where Im denotes the imaginary part, c is the speed of light, and $\alpha(\nu)$ is the polarizability of the nanoparticles.

Fig. 6 (Color online) Dichroic behavior of glass nanocomposite NC4: **a** brown in reflected light and **b** blue in transmitted light view (for composition see Table 1)



For a homogeneous spherical nanoparticle, the polarizability, $\alpha_s(\nu)$, is expressed by

$$\alpha_s(\nu) = \epsilon_m R^3 [\{\epsilon(\nu) - \epsilon_m\} / \{\epsilon(\nu) + 2\epsilon_m\}] \quad (4)$$

where R is the radius of the metal NPs, and $\epsilon(\omega)$ is the dielectric function.

Here, the optical absorption spectra have been measured by the UV–visible spectrophotometer for the nanocomposites containing 0, 0.007, 0.01, 0.02, 0.03 and 0.06 (wt%) of Ag. These are shown in Fig. 8. It gives a clear view of alteration of SPR bands with Ag concentration. Gonella et al. [37] have reported the broad Bi SPR band at around 400 nm and for silver also at around 400 nm in a dielectric medium with the refractive index 1.33 (i.e., in water). Therefore, bismuth and silver have identical surface plasmon frequencies in the identical dielectric medium and refractive index.

In this study, the base glass (0 wt% Ag) has shown a very weak broad SPR band range of 500–700 nm in Fig. 8a, and it could be attributed to SPR of Bi⁰ NPs. But when 0.007 and 0.01 wt% of silver are added to the glass, a prominent SPR absorption peak is observed at 575 nm. It is, therefore, due to the in situ formation of silver nanoparticle in the bismuth glass. From the standard reduction potential (E°) data given in Table 2, it is known

Fig. 7 Various orientations of crystalline planes of bismuth-coated silver nanoparticles

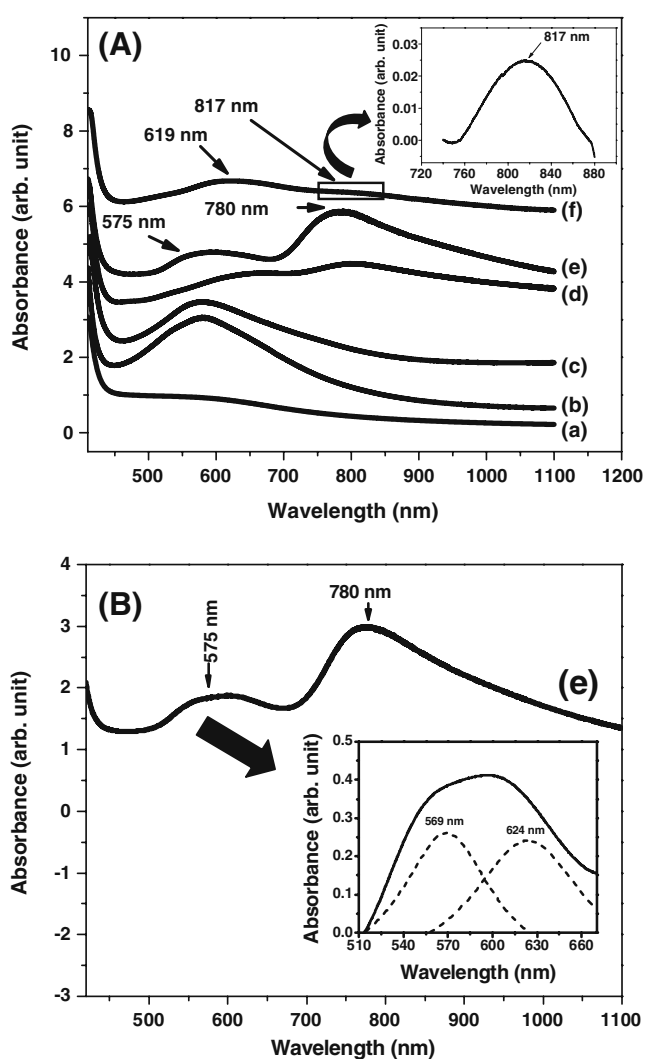
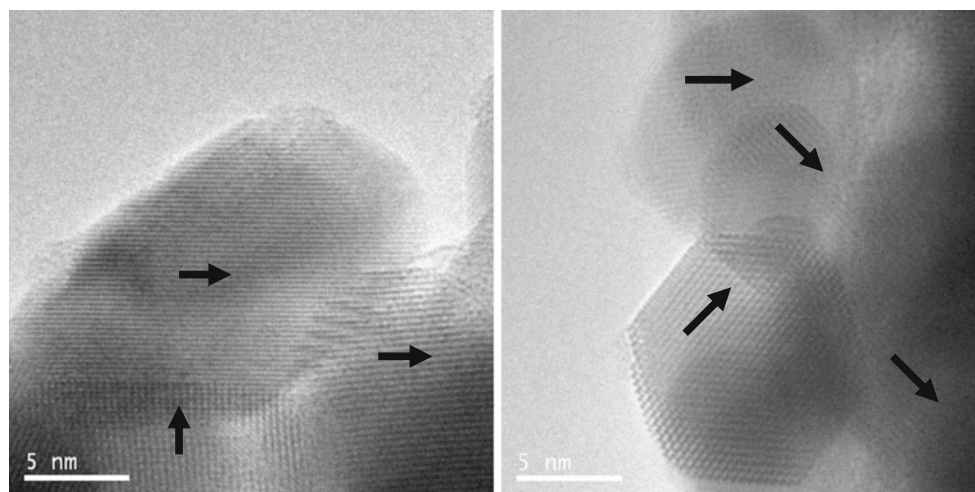
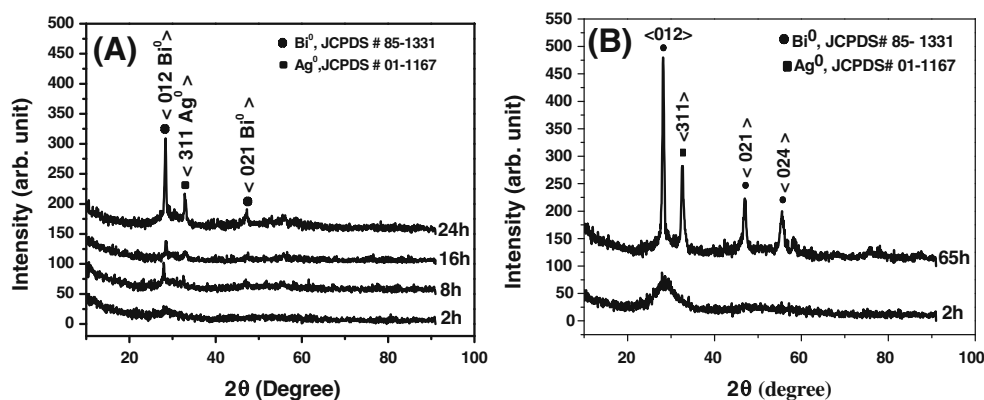


Fig. 8 **a** The absorption spectra of samples (a) G, (b) NC1, (c) NC2, (d) NC3, (e) NC4 and (f) NC5. *Inset* shows the second absorption peak of curve *f* at 817 nm (see Table 1 for composition). **b** *Inset* shows the deconvoluted spectral profile of first absorption band of the nanocomposites NC4 (see Table 1 for composition)

that silver was reduced earlier than that of bismuth and finally silver NPs being coated by the nanometallic bismuth layers. When the concentration of silver increased to 0.02 and 0.03 wt% in the glass, the SPR absorption band split into three peaks which are observed at 569, 624 and 780 nm. Figure 8b shows the deconvolution of the spectrum of the first absorption peak of sample containing 0.03 wt% of Ag (NC4). It is noted here that the SPR absorption band at 575 nm has been split into two bands, i.e., 569 and 624 nm. This observation indicates that at higher concentration of silver (0.02 and 0.03), the shape and size of the bismuth-coated silver nanoparticles have changed, and it was schematically represented in Fig. 1. The appearance of three bands causes for two reasons. Firstly, there may be presence of two or more types of particles, and secondly, existence of nonspherical NPs having three different resonances along three *x*-, *y*- and *z*-axes [38]. From the TEM image analysis, it is revealed that the spheroidal shape of NPs changes to hexagonal with the concentration of silver. The UV–vis absorption spectra, similar to nanorods and elliptical-shaped NPs, hexagonals, also showed two peaks, one peak for transverse mode excitation and the other for longitudinal mode of resonance [39]. The transverse (high energy) absorption band corresponds to electron oscillations perpendicular to the major axis, while the longitudinal (low energy) absorption band results from the oscillation of the electrons along the major axis [38]. Therefore, these three bands are assumed to be due to the presence of spheroidal (for the first band) as well as hexagonal NPs (for second and third bands) in these glasses.

Gans [39] predicted that for very small ellipsoids, where the dipole approximation holds, the surface plasmon mode would split into two distinct modes. He quantified the response as a function of the ellipsoid aspect ratio. Electron microscopy reveals that most nanorods are more like cylinders or sphero-capped cylinders than ellipsoids. How-

Fig. 9 X-ray diffraction spectra of sample (a) NC1 and (b) NC4 after heat treatment at 360 °C for different duration (hours) show various $\langle hkl \rangle$ planes of rhombohedral Bi^0 NPs (JCPDS file no. 85-1331) and cubic Ag^0 (JCPDS file no. 01-1167) (for composition see Table 1)



ever, an analytical solution for such shapes is not possible. Solutions have been found for the case of an infinite cylinder and for oblate and prolate ellipsoids. For non-spherical particles, better agreement with experiment is achieved using numerical approaches, such as the discrete dipole approximation (DDA) [40, 41] which has been applied extensively by Schatz and coworkers to study noble-metal clusters [42]. For smaller particles density functional theory (DFT), calculations can be used to obtain more accurate simulations of plasmon spectra [43]. In order to explain the optical properties of such nonspherical particles, it has been common to treat all such nonspherical as an ellipsoid, which allows the Gans formula to be applied. According to Gans, the polarizability of the ellipsoid particles, $\alpha_{x,y,z}$, can be represented as follows [44]:

$$\alpha_{x,y,z} = \frac{4\pi abc(\epsilon_m - \epsilon_{\text{med}})}{3\epsilon_{\text{med}} + 3L_{x,y,z}(\epsilon_m - \epsilon_{\text{med}})} \quad (5)$$

where a , b and c are the length of the ellipse along the x -, y - and z -axes ($a > b = c$), ϵ_m is the dielectric function of metal, ϵ_{med} is the dielectric constant of the medium at

optical frequencies, and $L_{x,y,z}$ is the depolarization factor for the respective axis, which is given by [42]

$$L_x = \frac{1 - e^2}{e^2} \left(-1 + \frac{1}{2e} \ln \frac{1+e}{1-e} \right) \quad (6)$$

$$L_{y,x} = \frac{1 - L_x}{2} \quad (7)$$

where e is the rod ellipticity which is expressed by $e^2 = 1 - (b/a)^2$. For a sphere, $e=0$ and $L=1/3$.

When 0.06 wt% of silver (NC5) is added to the bismuth glass, two red-shifted absorption bands are observed at 619 and 817 nm. This red shift indicates the increase in the particle size of hexagonal-shaped NPs with the increase in the concentration of metallic silver (Ag^0) in the glass nanocomposites. Similar observations have been reported by various authors [1–5].

Thermal Effect on the Bismuth-Coated Silver Nanoparticles

The two samples of NC1 and NC4 (see Table 1 for composition) are heat-treated at 360 °C for different time duration, and their respective XRD patterns are shown in

Fig. 10 a TEM image of the nanocomposites NC1 and b its SAED image after thermal treatment at 360 °C for 16 h (see Table 1 for composition)

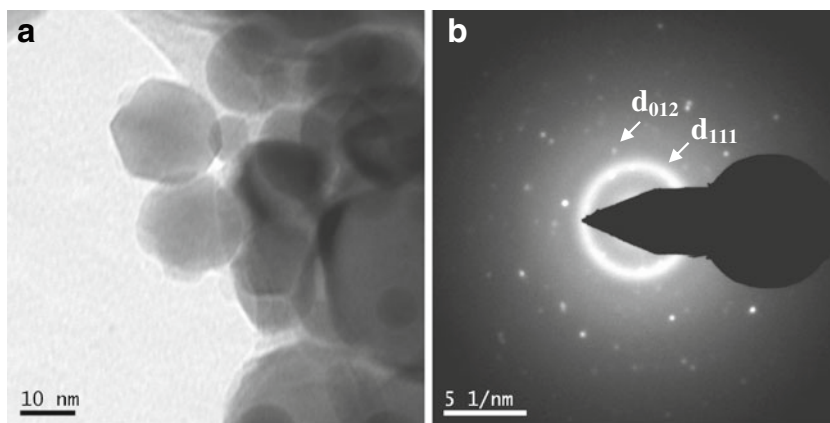


Fig. 11 **a** TEM image of the glass NC4 and **b** its SAED image after thermal treatment at 360 °C for 65 h (see Table 1 for composition)

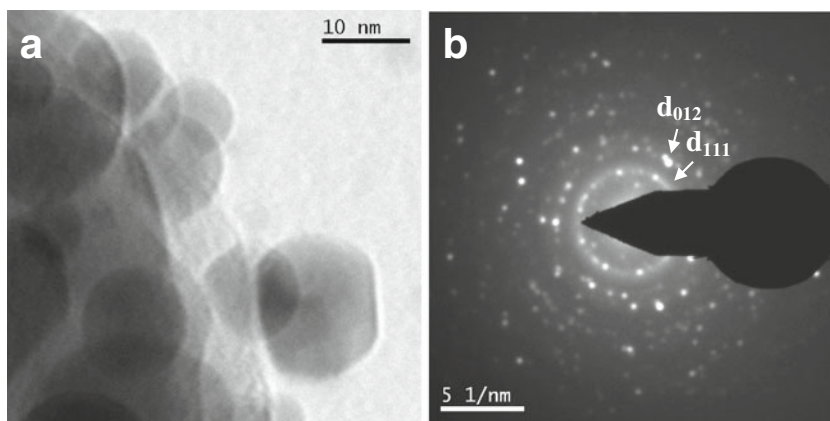


Fig. 9. XRD patterns reveal the presence of crystalline planes of rhombohedral bismuth and cubic silver. In both cases, it shows that the formation of metallic bismuth and silver increases continually with the heat treatment time. The sample NC4 shows two distinct crystalline hkl planes <021> and <024> of rhombohedral bismuth at 46.9 and 56.3° (JCPDS file no. 85-1331) when sample was heat-treated for 65 h (see Fig. 9b). Therefore, it is concluded that with the heat treatment, new crystalline planes of Bi⁰ are developed.

The effect of heat treatment on the morphology of the NPs has been analyzed by the help of TEM images. Figure 10a shows the TEM images of the NC1 glass nanocomposites which were heat-treated for 16 h at 360 °C. The sizes of NPs have increased (10–15 nm) in comparison to as-prepared sample (5–8 nm). It may be due to the further formation of nanoclusters by thermal effect. This fact can also be evidenced from the XRD analysis of heat-treated sample of NC1 (see Fig. 9a), which shows gradual formation of bismuth and silver nanometal with the heat treatment time. The thermal treatment effect on hexagonal-shaped NPs (NC4) was also examined (Fig. 11a), and interestingly, the shape of the NPs changes toward spherical when heat-treated at 360 °C for 65 h. The size of NPs also decreases to 10–20 nm. The XRD analysis of heat-treated sample of NC4 (see Fig. 9b) for 65 h shows the development of two distinctly new crystalline hkl planes <021> and <024> of rhombohedral bismuth (JCPDS file no. 851331). So, these planes may be causes for changes in the shape to attain the lowest energy (spheroidal) from high energy state (hexagonal) of NPs. The corresponding SAED images (Figs. 10b and 11b) show the presence of rhombohedral bismuth and cubical silver phases. The outer SAED ring correspond to <012> <hkl> plane of rhombohedral bismuth (JCPDS file no. 85-1331), whereas the inner electron diffraction pattern ring shows the <111> <hkl> planes of cubic silver (JCPDS file no. 01-1667) phases, respectively.

Here, we also investigated the thermal effect on the SPR due to bismuth-coated silver nanoparticles for the NC1 and NC4 samples. The absorbance spectra of heat-treated

samples of NC1 at 360 °C for 2, 8, 16 and 24 h are shown in Fig. 12. It gives a clear view of SPR band shift due to thermal effect on the spherical particles. The thermal effect shows very remarkable red shift of SPR in the range of 606 to 647 nm. This observed red shift causes the increase in nanoparticles size, and such results have also been reported by the several authors [45–47]. Such tuning of SPR band is very useful for the various applications in the field of sensor, photonics, etc. The average radius of the metal nanocluster, *r*, can be determined theoretically from the UV–visible absorption spectra by using the following equation [48, 49]

$$r = \nu_r / \Delta\omega \tag{8}$$

where ν_r is the Fermi velocity for metal, and $\Delta\omega$ is the bandwidth at half maximum (FWHM) of the plasmon resonance absorption band. The value of $\Delta\omega$ is determined using $\Delta\omega = 2c\pi(1/\lambda_1 - 1/\lambda_2)$, where *c* is the velocity of light

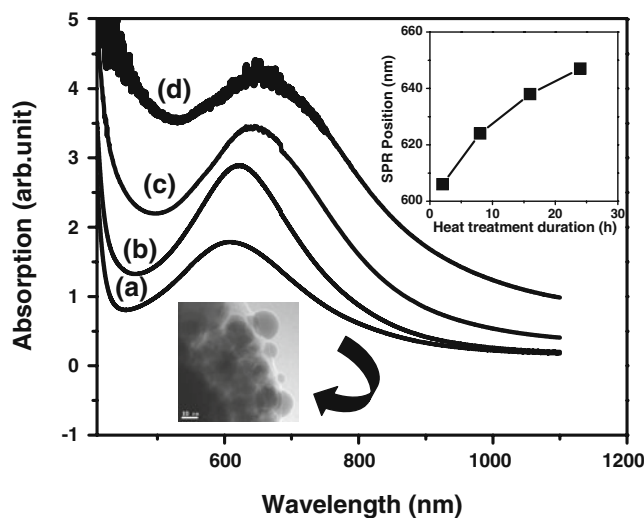


Fig. 12 UV–vis absorption spectra of NC1 after heat treatment at 360 °C for (a) 2, (b) 8, (c) 16 and (d) 24 h. Insets show the red shifting of SPR bands with the duration of heat treatment and the TEM image of a (for composition see Table 1)

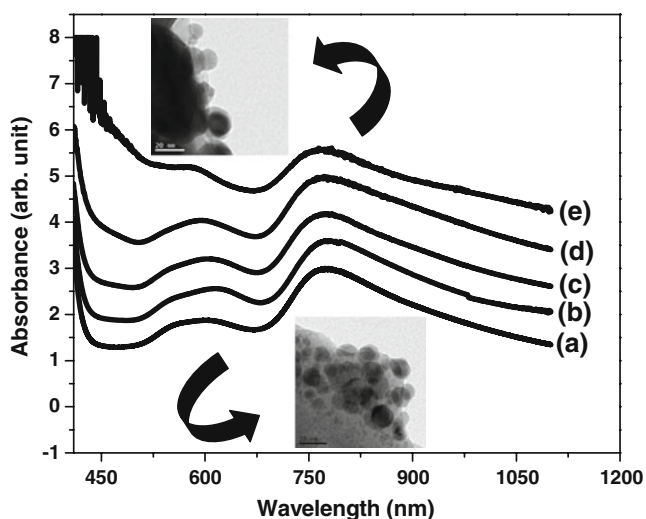


Fig. 13 UV-vis absorption spectra of NC4 after heat treatment at 360 °C for (a) 0, (b) 12, (c) 24, (d) 40 and (e) 65 h. Insets show the respective TEM images of the absorption spectra a and e (for composition see Table 1 and for SPR band position see Table 3)

in vacuum, and λ_1 and λ_2 are the wavelengths at FWHM. Figure 12 reveals that the value of $\Delta\omega$ gradually decreases with heat treatment time. As the value of ν_r is the same for all NPs, so the particle size increases with the heat treatment time. This is well correlated with the XRD and TEM analysis of heat-treated sample (please see Figs. 9a and 10a).

The SPR bands of sample NC4 after heat treatment at 360 °C for 12, 24, 40 and 65 h are also shown in Fig. 13. It gives a clear view of the alteration of SPR bands due to thermal effect on hexagonal particles. The as-prepared sample of NC4 shows three absorption bands at 553, 612 and 775 nm (see Table 3). The absorption bands at 553 and 612 nm are not well resolved (see Fig. 13). During heat treatment at 360 °C for 65 h, these two bands gradually merged into one weak band at 582 nm. But the absorption peak at 775 nm remains unchanged throughout heat treatment. This type of spectral change indicates the change in the shape and size of the NPs. From TEM analysis of heat-treated sample of NC4, it is clearly demonstrated that the change in shape toward spherical and decrease in the size in the range of 10–20 nm.

Table 3 Variation of SPR band position with heat treatment at 360 °C of sample NC4

Sample identity ^a	Heat treatment duration (h) at 360 °C	Position of SPR peak (nm) ^a		
		I	II	III
G	0	553	612	775
NC1	12	552	616	775
NC2	24	549	604	769
NC3	40	–	594	772
NC4	65	–	582	767

^a Please see Fig. 8 for SPR peak position (for composition, see Table 1)

Conclusions

Here, the synthesis of bismuth-coated silver nanoparticles by a novel simple melt-quench technique in the K_2O – Bi_2O_3 – B_2O_3 (KBB) glass matrix without employing any external reducing agent has been demonstrated. The glasses are dichroic in nature as they exhibit two different colors (brown in reflection and blue in transmission view). The XRD pattern shows metallic bismuth and cubic silver crystalline planes. TEM images demonstrate the presence of two types of NPs. It shows interestingly the evolution of spheroidal- to hexagonal-shaped NPs with increase in concentration (0.007 to 0.03 wt%) of silver and the NP size varying in the range of 5–8 to 10–35 nm. HRTEM images of the NPs show various orientation which is a responsible factor for the dichroic nature of the glass. FESEM images show house of hexagonal disk-like nanostructure in the glass. This fact is supported by TEM analysis as well. The TEM images of sample doped with 0.007 wt% of silver show the increase in particle size (10–15 nm) with the duration of thermal treatment. But the TEM images of the sample doped with 0.03 wt% of silver demonstrate the change in the hexagonal shape of NPs to spheroidal after heat treatment for 65 h. The UV-vis absorption spectra show single SPR absorption bands at lower concentration of silver (up to 0.01 wt% Ag) due to spheroidal shape of NPs. The glasses doped with 0.02 and 0.03 wt% of silver show three absorption bands which indicate two types of particles, i.e., spheroidal and hexagonal. Whereas at the highest concentration of silver (0.06 wt%), it shows two absorption bands due to hexagonal NPs. The SPR bands of heat-treated sample of 0.007 wt% of silver-doped glass show red shift with increase in time of heat treatment. This red shift is attributed to the increase in particle size. The sample doped with 0.03 wt% of silver shows unchanged absorption peak at 775 nm. But the other two peaks at 553 and 612 nm merge into one peak at around 594 nm. We believe that such a convenient and optimized synthesis method of Bi-coated Ag NPs will certainly benefit the field of nanoscience and nanotechnology. This work will open up a new approach in the field of nanoresearch as it

has potential applications in the area of nanophotonics and optoelectronics.

Acknowledgments SPS express his sincere gratitude for the financial support of the Council of Scientific and Industrial Research (CSIR), New Delhi in the form of CSIR-SRF under sanction number 31/15(78)/2010-EMR-I. The authors thank Prof. Indranil Manna, Director of the institute for his kind permission to publish this paper. We also thankfully acknowledge the XRD and Electron Microscope Divisions of this institute for recording the XRD, TEM, SAED and FESEM images.

References

- Bréchnignac C, Houdy P, Lahmani M (2007) *Nanomaterials and nanochemistry*. Springer, Berlin
- Ferrando R, Jellinek J, Johnston RL (2008) Nanoalloys: from theory to applications of alloy clusters and nanoparticles 108: 845–910
- Schiffrin DJ (2004) *Faraday discussions: nanoparticle assemblies*, vol 125. RSC, Cambridge
- Rao CNR, Müller A, Cheetham AK (2004) *The chemistry of nanometals: synthesis, properties and applications*, vol 2. Wiley, Weinheim
- Corain B, Schmid G, Toshima N (2008) *Metal nanoclusters in catalysis and materials science: the issue of size control*. Elsevier, Amsterdam
- Houk RJT, Jacobs BW, Gabaly FEI, Chang NN, Talin AA, Graham DD, House SD, Robertson IM, Allendorf MD (2009) *Nano Lett* 9:3413–3418
- Sherry LJ, Jin R, Mirkin CA, Schatz GC, Duyne RPV (2006) *Nano Lett* 6:2060–2065
- Choi B-h, Lee H-H, Jin S, Chun S, Kim S-H (2007) *Nanotechnology* 18:075706-1-5
- Konta R, Kato H, Kobayashi H, Kudo A (2003) *Phys Chem Chem Phys* 5:3061–3065
- Huxter VM, Scholes GD (2009) *J Nanophotonics* 3:032504-1-15
- Magruder RH III, Robinson SJ, Smith C, Meldrum A, Halabica A, Haglund RF Jr (2009) *J Appl Phys* 105:024303-1-5
- Bhattacharyya S, Bocker C, Heil T, Jinschek JR, Höche T, Rüssel C, Kohl H (2009) *Nano Lett* 9:2493–2496
- Benahmed AJ, Ho C-M (2007) *Appl Opt* 46:3369–3375
- Okamoto T, H'Dhili F, Kawata S (2004) *Appl Phys Lett* 85:3968–3970
- Scalora M, Bloemer MJ, Pethel AS, Dowling JP, Bowden CM, Manka AS (1998) *J Appl Phys* 83:2377–2383
- Stalmashonak A, Unal AA, Graener H, Seifert G (2009) *J Phys Chem C* 113:12028–12032
- An J, Tang B, Ning X, Zhou J, Xu S, Zhao B, Xu W, Corredor C, Lombardi JR (2007) *J Phys Chem C* 111:18055–18059
- Cobley CM, Skrabalak SE, Campbell DJ, Xia Y (2009) *Plasmonics* 4:171–179
- Blondeau JP, Veron O, Catan F, Kaitasov O, Sbai N, Andreazza-Vignolle C (2009) *Plasmonics* 4:245–252
- Zhang Y, Yang Y, Zheng J, Hua W, Chen G (2008) *J Am Ceram Soc* 91:3410–3412
- Sanz O, Haro-Poniatowski E, Gonzalo J, Navarro JMF (2006) *J NonCryst Solids* 352:761–768
- DeParis O, Mezzapesa FP, Corbari C, Kazansky PG, Sakaguchi K (2005) *J NonCryst Solids* 351:2166–2177
- Kustov EF, Bulatov LI, Dvoyrin VV, Mashinsky VM (2009) *Opt Lett* 34:1549–1551
- Cortie MB, Xu X, Ford MJ (2006) *Phys Chem Chem Phys* 8:3520–3527
- Vanýsek P (1994) *Electrochemical series*. In: Lide DR (ed) *CRC hand book of chemistry and physics*. CRC, London, p 22
- Ould-Ely T, Thurston JH, Kumar A, Respaud M, Guo W, Weidenthaler C, Whitmire KH (2005) *Chem Mater* 17:4750–4754
- Gutiérrez M, Henglein A (1996) *J Phys Chem* 100:7656–7661
- Katsikas L, Gutiérrez M, Henglein A (1996) *J Phys Chem* 100:11203–11206
- Michaelis M, Henglein A, Mulvaney P (1994) *J Phys Chem* 98:6212–6215
- Moore JT, Lukehart CM (2002) *J Mater Chem* 12:288–290
- Sun Y, Qiao R (2008) *Nano Res* 1:292–302
- Weyl WA (1951) *Colored glasses*. Society of Glass Technology, Sheffield, p 329
- Magruder RH III, Robinson SJ, Smith C, Meldrum A, Halabica A, Haglund RF Jr (2009) *J Appl Phys* 105:024303-1-5
- Mie G (1908) *Ann Phys (Leipzig)* 330:377–445
- Kreibig U, Quinten M (1994) In: Haberland H (ed) *Clusters of atoms and molecules*. Vol II. Springer, Berlin, p 321
- Kreibig U, Vollmer M (1995) *Optical properties of metal clusters*. Springer, Berlin
- Gonella F, Mazzoldi P (2000) *Metal nanocluster composite glasses*. In: Nalwa HS (ed) *Handbook of nanostructured materials and nanotechnology*. Vol 4. Academic, London, pp 81–101
- Hutter E, Fendler JH (2004) *Adv Mater* 16:1685–1706
- Gans R (1912) *Ann Phys* 37:881–900
- Amendola V, Bakr OM, Stellacci F (2010) *Plasmonics* 5:85–97
- Zhang JZ, Noguez C (2008) *Plasmonics* 3:127–150
- Kelly KL, Coronado E, Zhao LL, Schatz GC (2003) *J Phys Chem B* 107:668–677
- Bruzzone S, Arrighini GP, Guidotti C (2003) *Mater Sci Eng C* 23:965–970
- Jorge P'-J, Isabel P-S, Luis ML-M, Paul M (2005) *Coord Chem Rev* 249:1870–1901
- Jana NR, Gearheart L, Murphy CJ (2001) *Langmuir* 17:6782–6786
- Rodríguez-González B, Sánchez-Iglesias A, Giersig M, Liz-Marzán LM (2004) *Faraday Discuss* 125:133–144
- Moores A, Goettmann F (2006) *New J Chem* 30:1121–1132
- Arnold GW (1975) *J Appl Phys* 46:4466–4473
- Sheng J, Kadono K, Yazawa T (2003) *J NonCryst Solids* 324:295–299